# Spark-Gap Atomic Emission Microscopy

**P. G. Van Patten, J. D. Noll, and M. L. Myrick***

*Department of Chemistry and Biochemistry, University of South Carolina, Columbia, South Carolina 29208*

**C. R. Li and T. S. Sudarshan**

*Department of Electrical Engineering, University of South Carolina, Columbia, South Carolina 29208*

*Received: June 6, 1995; In Final Form: November 15, 1995*[⊗]

A new technique allowing elemental analysis of small regions of scanning tunneling microscopy (STM) substrates without loss of tip-surface registry has been developed. The technique is based on spark atomic emission spectroscopy and provides information normally unavailable from the STM. In this technique, a voltage excursion (>100 V) is used to excite the sample and cause emission. Spectra from a polished copper electrode surface are presented and discussed. Important parameters and present limitations are also discussed along with future directions for the improvement and long-term use of the technique.

## Introduction

Scanning probe microscopy (SPM) has in recent years revolutionized surface science by allowing enormous advances in surface imaging technology. Scanning tunneling microscopy[1] (STM) is the most commonly used type of SPM used for the imaging of metals and semiconductors. Though state-of-the-art instruments allow imaging of surface features with extremely high resolution (<1 nm), drawbacks are inherent in the technique. In particular, the images obtained lack any compositional or chemical information.

Efforts have been made to use the tunneling characteristics (for example through tunneling spectroscopy[2] or through the appearance of atomic-scale features in STM images[3−8]) of different materials to distinguish between them. Nevertheless, the ability to simultaneously image topography and verify chemical or elemental composition with independent, non-topographic means has thus far been elusive. This deficiency of STM has prompted our attempt to modify the instrument to allow *in situ* elemental analysis of the surface being imaged.

The technique of spark-gap atomic emission spectroscopy[9] (AES) seems readily adaptable to the configuration of the STM experiment. Spark-gap AES is a well-developed, well-understood technique which yields qualitative elemental analysis and straightforward, unambiguous spectra that are easily interpretable.

In this method, atomic emission is produced by creating a high-voltage discharge between two electrodes (one of which is often the sample). The power dissipated during the spark vaporizes, atomizes, and excites the sample to higher electronic states. The relaxation of the sample atoms is observed as emission of photons whose energies are characteristic of the sample.

In order to adapt the technique to STM, the sample is used as one electrode while the probe tip serves as the counter electrode. A high-amplitude bias pulse (∼150 V) is used to induce a visible spark. Collection of the emitted light into a spectrometer equipped with an intensified charge-coupled device array allows spectral analysis and identification of the elements present in the sample directly below the tunneling tip.

Due to the extreme proximity of tip and sample, relatively low voltages may be used for spark formation. A low voltage allows the sampling of a very small (a few $\mu m^3$) region, and thus high resolution. This is an important aspect of the experiment, as it allows the microscopist the opportunity to chemically sample individual structures encountered while imaging a surface without interference from neighboring structures.

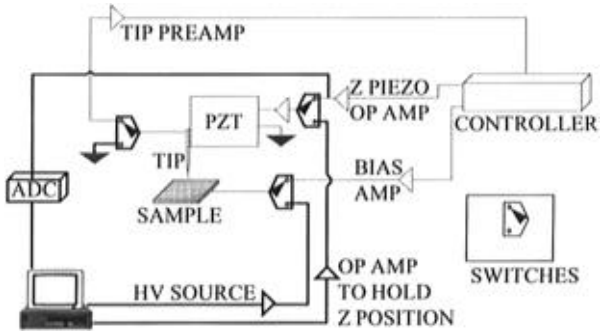


**Figure 1.** Electronic modifications (bold black lines) to existing STM hardward (gray lines) necessary to perform spark-gap atomic emission microscopy.

It should be pointed out here that this technique is quite unrelated to the photon emission scanning tunneling microscope developed by Berndt et al.[10,11] That instrument detects photons emitted in ultrahigh vacuum as a result of the excitation of surface plasmons through inelastic tunneling. The present technique probes the energy transitions between states of the free atom and tells nothing (other than elemental composition) about the bulk solid or surface from which the atom was ablated. Furthermore, this technique does not require highly crystalline samples, ultrahigh vacuum conditions, or pristine surfaces.

## Experimental Section

Our apparatus (Figures 1 and 2) consists of a Digital Instruments Nanoscope II modified to allow application of brief (∼$10^{-3}$ s), high-amplitude voltage pulses between tip and substrate. This results in a series of transient (∼$10^{-6}$ s) electron avalanches in the gap (see Figure 3). High voltage is produced by an operational amplifier with a ±145 V output capacity. An analog switch selects between this amplifier and the normal bias amplifier. A mercury-wetted relay is placed in the circuitry to prevent this high voltage from reaching the tip preamplifier and damaging it. Another operational amplifier and switch are used

[⊗] Abstract published in *Advance ACS Abstracts,* January 15, 1996.

0022-3654/96/20100-3646$12.00/0 

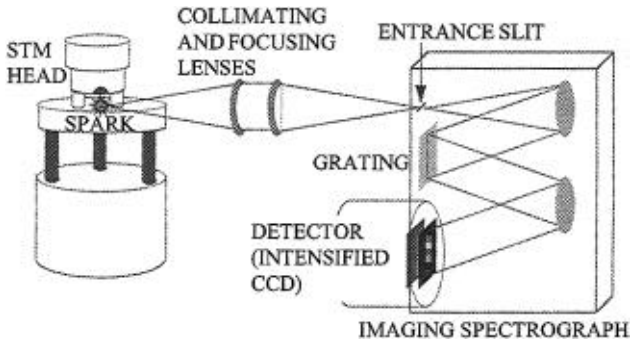


**Figure 2.** Optics arrangement for spectral analysis of high-voltage spark.

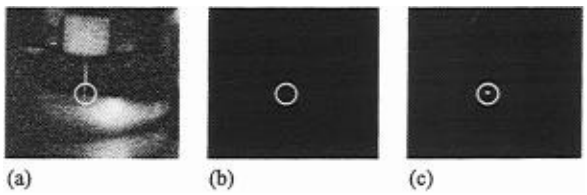


**Figure 3.** (a) Image of STM tip under normal tunneling conditions. The circle indicates the position of the tunneling gap. (b) Same area, without illumination. (c) 130 V spark between tip and surface.

to seize control of the *Z* piezoelectric scanner and immobilize it. This prevents the feedback loop from retracting the tip during the experiment. The $X-Y$ position of the tip is held constant during the experiment by setting the STM scan size to 0 nm. (Though we have no quantitative measure of the $X-Y$ drift that occurs during a voltage pulse, evidence from postspark images indicates that the drift is small compared to the size of the blast craters.)

The electronic modifications are controlled by a second computer. After the protection relay is switched to prevent preamp damage, a voltage pulse is applied to the operational amplifier. The operational amplifier is then selected by the appropriate analog switch to apply the voltage to the sample. The reverse procedure returns the instrument to normal tunneling operation.

All spectroscopic experiments were carried out in air using a scan head with a maximum scan range of 100 $\mu$m × 100 $\mu$m. The discharge voltage used was −130 V (applied to the substrate) and was maintained for 10−100 ms. Some experiments were performed in which the substrate served as the anode, but no spectroscopy has yet been performed in this mode. In all cases, the substrate used was Cu metal or highly oriented pyrolytic graphite (HOPG) and the tip was W metal wire. The tips used for determination of tip erosion were etched electrochemically in a 1 M NaOH solution with a platinum counter electrode and an applied ac voltage of ∼10 V. In all other experiments the tips were cut with wire cutters.

The spectrometer was a SPEX 270M (f4 optics) with a 300 g/mm grating. The detector was a thermoelectrically cooled intensified CCD array by Stanford Computer Optics, Inc., triggered on the rise of the discharge voltage.

Images of the tip shown in Figure 3 were captured using a Vicon CCD video camera fitted with a custom Vicon lens ordered specifically for viewing STM tips.

## Results

During a 130 V, 100 ms bias pulse, light emission can be observed at the tunneling tip. This is illustrated in Figure 3 which shows (a) the tunneling gap under normal circumstances, (b) the tunneling gap without illumination while tunneling, and (c) the tunneling gap during sparking in the absence of external illumination.

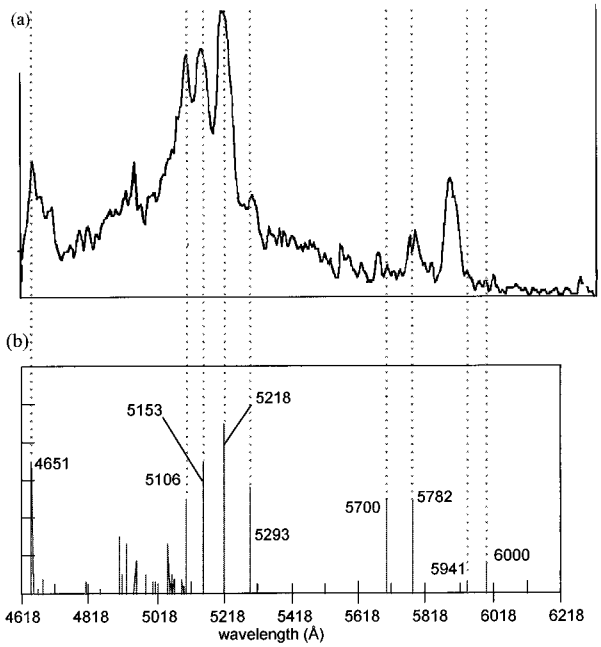


**Figure 4.** (a) Spectrum of spark obtained during 100 ms, 130 V voltage pulse. (b) Simulated spectrum of Cu(I) from tabulated data. Many of the other peaks in the spectrum can be ascribed to interferents such as W (the tip material) or N (from the air).

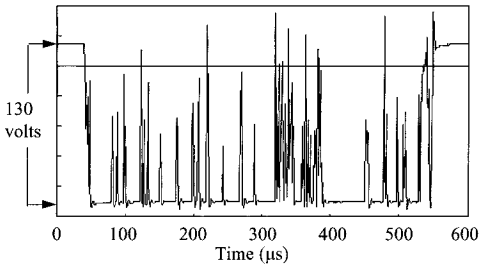


**Figure 5.** Digital oscillogram of a 0.5 ms, 130 V spark showing peaks which correspond to individual electron avalanches across the tunneling gap. These current surges typically last 1−2 $\mu$s. Experiments with simultaneous PMT recording show that photons are emitted only during these brief current surges.

When performed above a copper electrode, the spark appears green to the eye. A spectrum of this copper emission has been obtained and is shown in Figure 4a. Figure 4b shows a copper line spectrum generated from a table of atomic line intensities, showing all Cu I (neutral copper) lines appearing in this wavelength region.

A trace of voltage versus time during a voltage pulse is shown in Figure 5. At several points during the event, the voltage can be observed to collapse back to zero. A synchronous plot of output from a photomultiplier tube verifies that light emission is observed only during these transient voltage collapses. These collapses can occur several times per millisecond, as shown in the Figure. The optical events associated with these voltage collapses average about 800 ns in duration.

We interpret each of these transient voltage collapses as individual breakdown events. During these events, the resistance of the gap becomes very small, and the current, very large. The amplifier supplying the voltage is incapable of maintaining the voltage under these conditions, and thus it drops to zero also. In the absence of the initiating voltage, the spark terminates, allowing the voltage to return to 130 V.

Figure 6 shows (a) a trace of one of these voltage collapses with higher time resolution and (b) a synchronous plot of current

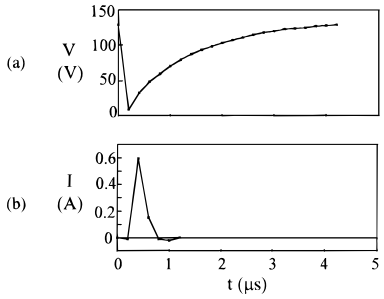


**Figure 6.** (a) Bias voltage as a function of time during an individual breakdown event, showing typical RC charging behavior. (b) Synchronous current measurement.

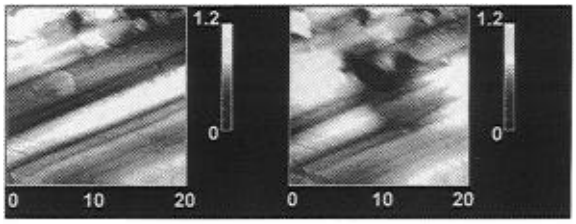


**Figure 7.** 20 × 20 $\mu$m STM scan of a polished copper electrode surface (a) before and (b) after a 100 ms, 130 V spark.

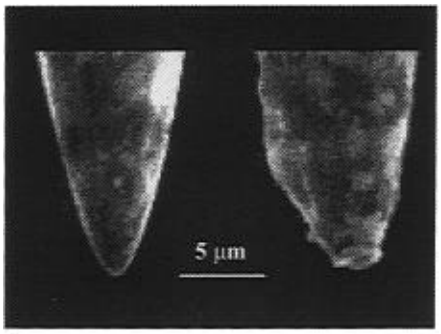


**Figure 8.** Scanning electron micrographs of an etched tungsten tip (a) before and (b) after a 130 V, 100 ms spark. The radius of the damaged region is approximately 1.5 $\mu$m.

during the same transient, illustrating that the current indeed increases greatly during one of these transients. The voltage trace exhibits behavior typical of an RC circuit, with an exponential charging curve. Due to the unknown resistance of the tip, the true potential at the capacitor (tunneling gap) cannot be known exactly. Nevertheless, the current measurement should be unaffected by the capacitance of the system and should be reliable. The maximum current measured in Figure 6 was about 650 mA. Unfortunately, the capacitive nature of the gap makes a determination of power dissipation across the gap impossible with the data obtained to this point.

Figure 7 shows a 20 × 20 $\mu$m image of a polished copper electrode (a) before and (b) after a 130 V, 100 ms voltage pulse that generated a visible spark. The ablated region covers an area of approximately 10 $\mu m^2$ and is measured (by the dulled tip) as being approximately 1.5 $\mu$m deep at the deepest point.

The damage done to a tungsten tip during a similar pulse sequence is shown by the SEM images in Figure 8a,b. This tip was prepared by etching to achieve a shape that was smooth and radially symmetric.

Figure 9 shows an STM image of two converging HOPG ledges imaged after pulsing the tip for 100 ms at 130 V. This image serves to quantify the optimum resolution after a sparking

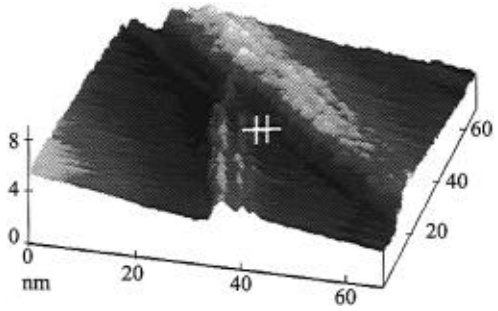


**Figure 9.** Image demonstrating the ability to obtain high-resolution images even after sparking with the tip. Shown here is the convergence of two ledge defects on HOPG imaged with a 94.6 $\mu$m scan head and a W tip which has been used to generate a spark. The two crosses mark spots 3.80 nm apart. The ledges are resolvable to around 1 nm (the limit of the scan head). A 1 $\mu$m head with the same tip might achieve even higher resolution after sparking.

event. The two ledges are resolvable down to a separation of less than 1 nm. Of course, even if tips merely rearrange, but do not ablate, changes in imaging are expected at the atomic level. When this rearrangement occurs, one does not expect to observe identical images before and after sparking, even for tips that do not ablate and even when resolution is maintained.

The results outlined above clearly demonstrate that high-voltage pulses of 130 V are capable of generating visible sparks. Furthermore, the light emitted carries the atomic lines of the elements present on the substrate. Comparison of the spark spectrum in Figure 4a with the Cu I lines in Figure 4b allows easy identification of the material below the tip as copper. The similarities are most apparent in the progression of lines between 510.6 and 529.3 nm, but two lines at 465.1 and 578.2 nm also aid in identification. Most of the other peaks present can be ascribed to the presence of nitrogen (from the air) and tungsten (from the tip). For many elements, the presence of a single, well-resolved line is sufficient for identification, as exact overlaps are rare. Use of multiple lines, however, relaxes constraints on spectral resolution and thus improves detectability.

Gated detection schemes are frequently used to improve signal-to-background ratios in plasma emission measurements that demonstrate strong temporal dependence. No such measurements have yet been attempted, but evidence from other laboratories suggests that improved measurements could be made in this way.[12]

Normally, a spark's temperature can be estimated experimentally by comparing the intensity of emission from ionized species with that from neutral atoms. A Boltzmann distribution is assumed, and the temperature calculation is relatively straightforward. Such a calculation is impossible in these experiments. Due to the high field present, the time required for the removal of $Cu^+$ (<1 ns) is several orders of magnitude shorter than the excited state lifetimes of these species. Therefore, even if the spark were to produce significant numbers of charged particles, the probability of observing emission from them would remain quite slim.

## Discussion

Since the feedback loop of the STM is defeated during the pulse sequence, the possibility of tip−surface contact exists. Brief contacts between tip and surface would result in short circuits, possible light emission, and the observation of brief voltage collapses.

Thermal and vibrational displacement of the tip, for example, could result in tip crashes during the experiment. The danger of drift-related tip crashes has been minimized by a slight (~8

nm) retraction of the tip during the experiment. Frequency of crashes resulting from thermal drift or vibration during the brief interruption of the servomechanism should be nearly independent of the bias voltage applied to the tip. The absence of such crashes during low-voltage pulses (<35 V) offers evidence that tip crashes are not the cause of the observed voltage collapses during high-voltage pulses.

Electrostatic attraction between tip and surface is another factor which could cause tip crashes during a pulse sequence. An idealized tip (see tunneling gap model below) charged to 130 V and only 1.0 nm away from the substrate would experience an attractive force of approximately 18 $\mu$N. Though a substantial stress, it is not enough to significantly strain the tip. The elastic modulus of tungsten is approximately 345 GPa[13]. On a 1 cm long tip of 200 $\mu$m diameter, then, the tip could be expected to extend only about 2 Å. Though the strain can be expected to be somewhat longer due to the thinning of the tip near the end, this value is ~2 orders of magnitude smaller than the width of the gap during pulses and we feel it is reasonable to neglect this effect in a first approximation.

Since direct tip−surface contact appears unlikely, it is concluded that the voltage collapses must be indicative of breakdown events.

A mathematical model of the process has been constructed for the purposes of estimating the total field emission current. We begin by modeling an idealized tunneling gap for the purposes of the model. We approximate the tip as a hyperboloid given by

$$z\ (\text{nm}) = [r^2 + 100]^{1/2} \tag{1}$$

in cylindrical coordinates, where $z$ and $r$ are in nanometers. The substrate is assumed to be $z = 0$, or the r-plane (see Figure 12). This gives a minimum gap length of 10 nm, probably not an unreasonable estimate with tip retraction.

The field strength at the electrode surface is a function of position, but an analytic expression can be derived for this variable. For cold metal electrodes in intense electric fields, the Fowler−Nordheim (F−N) field emission equation is usually invoked to give approximations of current density. The equation is most commonly given in the form

$$J = \frac{1.541 \times 10^{-6} E^2}{\phi t^2(y)} \exp\left\{-6.831 \times 10^7 \frac{\phi^{3/2}}{E} v(y)\right\} (\text{A/cm}^2) \tag{2}$$

where $E$ is the electric field (V/cm), $\phi$ is the work function of the cathode (eV), and $t(y)$ and $v(y)$ are functions describing the magnitude of the tunneling barrier.[14] The value of $y$ is given by

$$y = 3.795 \times 10^{-4} E^{1/2}/\phi \tag{3}$$

with the functions $t$ and $v$ being corrections which account for the image field effect.

An interesting consequence of the Fowler−Nordheim theory is that when $y = 1$, the barrier maximum, ($\beta_{max}$) dips to the Fermi energy. For any value of $y > 1$, electrons whose component of kinetic energy normal to the metal surface ($E_x$) exceeds $\beta_{max}$ experience barrierless emission, as shown in Figure 10. This gives rise to a nontunneling field emission (NTFE) current. For a W cathode ($\phi = 4.65$ eV) barrierless emission occurs when $E$ exceeds 15 GV/m. The maximum field generated in these experiments is in this range, so NTFE could be observed in some cases in those regions with very small values of $r$. When NTFE occurs, breakdown should be observed as soon as a critical value of electric field is established. In regions where breakdown results from a long series of electron avalanches, a time lag should be observed between field establishment and breakdown. Evidence supporting the phenomenon of NTFE was obtained and is presented in a subsequent section.

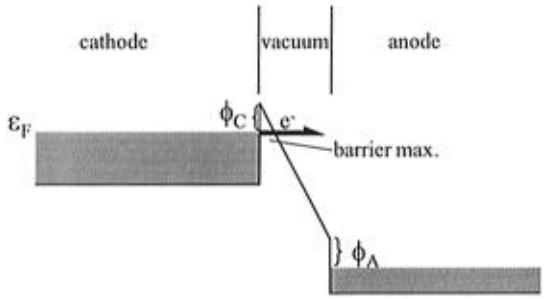


**Figure 10.** One-dimensional, one-electron model of nontunneling field emission into vacuum. As the field is increased, the image potential drops the barrier maximum below the Fermi energy, $\epsilon_F$. Electrons near the Fermi energy then experience barrierless emission into the vacuum gap.

The total instantaneous field emission current between the electrodes has been estimated in the field-emission regime $E <$ 1.50 V/Å by evaluating $J$ in the $F-N$ equation for different values of $r$ and integrating numerically over the surface area of either electrode. By this method, the maximum current density (at $r = 0$) has been calculated to be ~2 GA/cm$^2$. The total field emission current has been calculated as ~15 mA, which is sustainable by the high-voltage amplifier used. Field emission alone, then, should not induce voltage collapse. During sparking, the current should greatly exceed this predicted field emission value.

Up to this point, no mention has been made of the polarity of the electrodes during sparking. At this point, we will assume that polarity of the spark is a minor consideration, as the work functions of the electrodes are essentially the same. Experiments indicate that the sparking voltage is independent of polarity for a Cu surface and W tip. In the following discussion, the tip will be the cathode, and high-energy electron impacts at the substrate will be responsible for sample excitation.

In order to produce the atomic (photon) emission desired, a certain minimum energy must be carried by the electron current. This energy is required to accomplish two things: (1) to atomize a portion of the substrate; (2) to raise the temperature to a level at which a significant fraction of the atoms populate excited states (typically several thousand degrees Kelvin).

Since, in these experiments, the applied bias is 130 V and the difference in work functions for the two metals (Cu and W) is negligible (~0.1 eV) by comparison, the kinetic energy given up by each electron upon impact with the anode is approximately 130 eV.

Using a Monte Carlo simulation for the trajectories of electrons as they penetrate into the metal, we estimate that the average penetration depth of electrons into the metal is less than 10 nm.[15] Noting that >99% of the current density occurs at $r <$ 20.5 nm, we can imagine a cylinder in the anode of $r = 20.5$ nm and height (depth) = 10 nm into which we will inject the kinetic energy of the first few incident electrons. Using these approximations, assuming adiabatic conditions, and ignoring the energy required for other processes, we can estimate that at least $10^4$ electron impacts are required to melt and then to vaporize this volume of Cu substrate (approximately 1 e$^-$/12 Cu atoms). At the extreme current densities predicted during the spark-gap pulse, the vaporization of Cu by electron impacts could be effectively instantaneous by any measure, the rate-limiting step being the minimum time required to apply the high voltage.

The result is that the electron cascade creates a plume of copper plasma between the tip and substrate which effectively short circuits the gap in a small fraction of a second. This plasma is the source of most of the photon emission observed during these experiments.

This mechanism of plasma formation is similar to that described by Kinsey[16] and a modification of Townsend's[17] mechanism for cases of very small electrode spacings. Townsend's mechanism consists of initial charge carriers (electrons) appearing in the gap (by field emission in this case) and accelerating down the potential gradient to very high kinetic energies before colliding with other particles. In the case of very small electrode spacings (less than $\sim 3$ $\mu$m), the first collision of the electron is likely to be with the anode. The high kinetic energy of the electron (130 eV in this experiment) is sufficient to eject secondary charge carriers (both electrons and metal atoms/ions) from the anode. After acceleration by the high field, these particles spawn their own cascades of secondary particles until, after a short time, an avalanche of charge carriers fills the gap, and the current becomes very high.

The damage sustained by the substrate during these experiments is of great importance. This parameter determines the optimum spatial resolution of the technique. The ablation of small areas of substrate via bias voltage excursions into the field emission regime is not new. In this lab, 30 V pulses have been used to induce craters 20−30 nm in diameter in HOPG substrates. However, these experiments have not been observed to produce sufficent light emission for spectral analysis.

The damage to the Cu electrode in Figure 7 extends out to around $r = 2.5$ $\mu$m or so. Though this does not result in outstanding spatial resolution, this resolution may be improved in several ways. The most obvious experimental parameters to adjust for resolution improvement are voltage, tip−sample separation, tip shape, and voltage pulse duration. Improved resolution is a primary goal in the further development of this technique.

Currently, there is no way to prescribe the number of voltage collapses that occur during a voltage pulse. The solution to this problem is a system that detects the first voltage collapse and immediately terminates the HV pulse. This would allow the user to minimize surface damage while assuring light emission in every experiment.

According to the tip shape assumed above, the gap distance z approaches r for large values of *r*. This means that at the edge of the crater formed in Figure 7, the spark length would be about 2.5 $\mu$m, a reasonable value for the maximum allowed spark length in this experiment.[16] It is possible, therefore, that the surface ablation is limited to that region which experiences high current and that radial heat conduction plays a minimal role in vaporizing copper.

In ref 16, Kinsey showed that, for very small spark gaps ($<$100 nm), condensation of the metal plasma can cause the electrodes to "cohere" or produce a microbridge which traverses the gap and short circuits the electrodes together. Oscilloscope traces indicate that this phenomenon may occur occasionally in our experiments. In these cases, the voltage remains low following a collapse until the feedback loop is restored, at which time this bridge is presumably torn apart. These cases are uncommon, though, and most experiments resemble the trace shown in Figure 5.

An important variable affecting the size of the area destroyed is the exact shape of the tip. The crater shown in Figure 7 shows that the damage was not radially symmetric, but elliptical. The oblong appearance of the crater probably reflects the natural shape of the tip. Sharper, more radially symmetric tips may decrease the current as well as the diameter of the spark "waist" and thus increase the spatial resolution of this technique. Tips which exhibit radial symmetry and extreme sharpness (tip solid angle = 12−30° compared to $\sim$90° for the cut tips assumed in this study) can be fabricated through etching and other techniques[18,19] and may be useful for this application. Results to date with etched tips show that tip shape does tend to affect resolution in a manner consistent with general expectation.

One other parameter must be considered in the attempt to minimize the extent of surface erosion during a spark discharge. As the size of the crater decreases, so does the sampling volume and thus the spectral signal. Thus, the signal-to-noise ratio may put an effective lower limit on the sampling volume.

Tip erosion is almost as important as surface erosion, since it could limit the ability to acquire further images after sparking and could cause spectral interference if tip material is vaporized and excited by the spark. Tip erosion is minimized by using tungsten (mp, 3683 K; bp, 5933 K) tips. We see from Figure 8b that significant damage is done to the tips during sparking. The observed change in shape is certain to change the sharpness of the tip and to laterally displace the exact position of the tunneling contact. Nevertheless we have succeeded in these experiments in obtaining high-quality postsparking STM images.

The resolution of the image in Figure 9 demonstrates that postspark imaging is possible with high resolution. The ledges are resolvable down to a separation of 1 nm. As this approximates the optimum resolution of the scan head being used in this image, this resolution may not be tip-limited. In most experiments, no visible degradation of image quality resulted from the sparking. Atomic resolution is probably not possible after a spark, but the ability to acquire high-resolution images after sparking seems to be the rule rather than the exception.

The final tip concern is that of lateral displacement of the tunneling gap due to the change in tip shape. Figure 7 gives insight to the extent and impact of this effect. As can be seen by comparing the images, the lateral displacement of the tunneling gap is typically small compared to the crater diameter. (No $X-Y$ tip translation was performed after this sparking event.)

**Nontunneling Field Emission.** NTFE is a predicted result of the image effect when extremely high fields ($>\sim 10^8$ V/cm) are present at the metal surface. However, it has not been explicitly mentioned or explored in the literature as far as we know. We have suggested the possibility of NTFE in the above discussion. Verification of the presence of this phenomenon would be difficult without extensive experimentation directed specifically toward that end. We have not attempted such verification in the present experiments but have obtained data that supports the possibility of NTFE.

Figure 11 shows an image of HOPG taken immediately after a 130 V pulse which lasted only a few microseconds. No voltage collapse occurred during the pulse. Nevertheless, minor damage was sustained by the surface in the form of a narrow trench which wanders randomly about the surface within a 1 $\mu$m$^2$ circle. The trench varies from $\sim$20 to 50 nm wide. This behavior seems to be consistent with the predicted phenomenon of NTFE.

The wander indicated in the image must be evidence of a wandering tip rather than merely a wandering discharge. It seems unlikely that the wander of the hole is due to an analogue of arc wander over an entire $\mu$m$^2$, a region where *z* varies from 10 to 500 nm. Wander of the tip could be caused by forces arising from the high-voltage, high-current-density event. The Coulombic attraction between tip and substrate was earlier

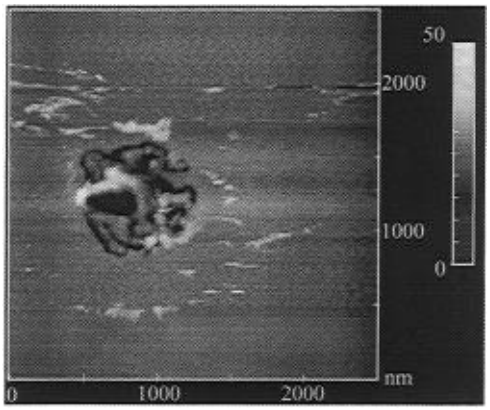


**Figure 11.** Damage done to HOPG during a 130 V pulse that lasted only a few microseconds. No voltage collapse was observed during the pulse. The narrow channel that appears could be the result of nontunneling field emission.

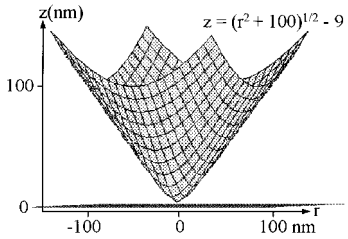


**Figure 12.** Illustration of the hyperboloid surface represented by eq 1. This is the assumed shape of the STM tip for the calculations performed in this paper.

estimated at about 18 $\mu$N. After the creation of a small asymmetric crater, the net torsion on the tip from the raised edges of the crater might be sufficient to deflect the tip slightly. If this occurred, the tip could be induced to etch out a pattern on the substrate with high-energy electrons, hence, the wandering trench of Figure 11.

## Conclusion

A prime focus of the future development of spark-gap atomic emission microscopy must be improvement of spatial resolution. The technique bears several advantages over other surface analysis techniques, and these have been outlined above. Slight improvements in spatial resolution are necessary, though, to make this technique competitive with the best existing techniques.

With a spatial resolution of a few $\mu m^2$, this technique is already competitive with scanning XPS and is slightly worse than diffraction-limited optical microspectroscopies. For many purposes, however, the elemental analysis possible with this technique is more valuable than the vibronic information available through the microscpectroscopies. Further progress in this field may well yield lateral resolution which matches or surpasses the diffraction limit. Currently, the highest lateral resolution in surface chemical analysis is available through scanning Auger electron spectroscopy, which has optimal lateral resolution of less than 50 nm. While it seems unlikely that atomic emission microscopy will surpass this mark, it is important to remember that scanning Auger has drawbacks of its own. It is an ultrahigh vacuum technique requiring expensive equipment and considerable expertise in spectrum analysis. Furthermore, locating a specific surface structure can necessitate the analysis of a large area, which consumes a great deal of time.

Thus, considering expense, ease of use, and practicality for STM users, atomic emission microscopy may be the best option.

The use of W tips appears to eliminate any serious problems with tip erosion. Though erosion occurs, continued imaging is possible and yields high-quality images.

**Acknowledgment.** Funding for this project was provided by the National Science Foundation (NSF) (Grant No. DMR-9207460). The authors would like to thank Dr. Norbert Bikales (NSF) for his support. The authors also wish to thank Dr. David C. Joy of the University of Tennessee, Knoxville, for providing the Monte Carlo simulation for electron beam−surface interactions.

## References and Notes

(1) Binnig, G.; Rohrer, H.; Gerber, Ch.; Weibel, E. *Phys. Rev. Lett.* **1982**, *49*, 57.

(2) Hansma, P. K. *Tunneling Spectroscopy: Capabilities, Applications, and New Techniques*; Plenum Press: New York, 1982.

(3) Venkataraman, B.; Flynn, G. W.; Wilbur, J. L.; Folkers, J. P.; Whitesides, G. M. *J. Phys. Chem.* **1995**, *99*, 8684−9.

(4) Stabel, A.; Heinz, R.; Rabe, J. P.; Wegner, G.; De Schryver, F. C.; Corens, D.; Dehaen, W.; Süling, C. *J. Phys. Chem.* **1995**, *99*, 8690−7.

(5) Jung, T.; Mo, Y. W.; Himpsel, F. J. *Phys. Rev. Lett.* **1995**, *74* (9), 1641−4.

(6) Sautet, P.; Dunphy, J. C.; Ogletree, D. F.; Jochim, C.; Salmeron, M. *Surf. Sci.* **1994**, *315*, 127−42.

(7) Patrick, D. L.; Beebe, T. P., Jr. *Langmuir*, **1994**, *10*, 298−302.

(8) Breen, J. J.; Flynn, G. W. *J. Phys. Chem.* **1992**, *96*, 6825−9.

(9) Ingle, J. D., Jr.; Crouch, S. R. *Spectrochemical Analysis*; Prentice Hall: Englewood Cliffs, NJ, 1988; Chapters 7−9.

(10) Berndt, R.; Schlittler, R. R.; Gimzewski, J. K., *J. Vac. Sci. Technol. B.* **1991**, *9* (2), 573−7.

(11) Berndt, R.; Gaisch, R.; Schneider, W. D.; Gimzewski, J. K.; Reihl, B.; Schlittler, R. R.; Tschudy, M. *Phys. Rev. Lett.* **1995**, *74* (1), 102−5.

(12) Luppi, R.; Pecorella, F.; Cerioni, I.*; Rev. Sci. Instrum.* **1984**, *55* (12), 2034−6.

(13) Van Vlack, L. H. *Elements of Materials Science and Engineering*; Addison-Wesley: Reading, MA, 1980; p 195.

(14) Gomer, R. *Field Emission and Field Ionization*; Harvard University Press: Cambridge, MA, 1961; Chapters 1 and 2.

(15) This number is the Bethe electron range calculated from a plural scattering Monte Carlo model. Though this model is not as accurate as the single scattering model, it is quite appropriate for the very low beam energy (0.13 keV) being used here. Copies of the programs for PC and MacIntosh, as well as additional information, are available from these authors as well as from Dr. Joy at the University of Tennessee, Knoxville.

(16) Kinsley, C. *Philos. Mag.* **1905**, *6* (9), 692.

(17) (a) Townsend, J. S. *Nature* **1900**, *62*, 340. (b) Townsend, J. S. *Philos. Mag.* **1901**, *1*, 198.

(18) Albrektsen, O.; Salemink, H. W. M.; Mørch, K. A.; Thölen, A. R. *J. Vac. Sci. Technol. B* **1994**, *12*, 3187−90.

(19) Fotino, M. *Rev. Sci. Instrum.* **1993**, *64* (1), 159−67, and references cited therein.

JP951540Z